

Breaking the Far-Field Diffraction Limit in Optical Nanopatterning via Repeated Photochemical and Electrochemical Transitions in Photochromic Molecules

Nicole Brimhall,¹ Trisha L. Andrew,² Rajakumar Varma Manthana,¹ and Rajesh Menon^{1,*}

¹*Department of Electrical and Computer Engineering, University of Utah, Salt Lake City, Utah 84112, USA*

²*Department of Chemistry, Massachusetts Institute of Technology, Cambridge, Massachusetts 02139, USA*

(Received 8 July 2011; published 7 November 2011)

By saturating a photochromic transition with a nodal illumination (wavelength, λ), one isomeric form of a small molecule is spatially localized to a region smaller than the far-field diffraction limit. A selective oxidation step effectively locks this pattern allowing repeated patterning. Using this approach and a two-beam interferometer, we demonstrate isolated lines as narrow as $\lambda/8$ (78 nm) and spacing between features as narrow as $\lambda/4$ (153 nm). This is considerably smaller than the minimum far-field diffraction limit of $\lambda/2$. Most significantly, nanopatterning is achieved via single-photon reactions and at low light levels, which in turn allow for high throughput.

DOI: 10.1103/PhysRevLett.107.205501

PACS numbers: 81.16.Rf, 42.50.St, 42.70.Jk, 81.16.Nd

Deterministic manipulation of matter at the nanoscale over macroscopic areas can lead to new material properties, enabling unique functionalities. However, patterning nanostructures over macroscopic areas remains challenging. As opposed to pattern replication, pattern generation is, in general, slow. Scanning-electron-beam lithography (SEBL), which is the dominant method for pattern generation at the nanoscale, is a serial, slow process. Also, electrons are readily deflected by extraneous electromagnetic fields, limiting the accuracy with which patterns can be placed relative to one another [1,2]. Patterning with photons, on the other hand, can be fast due to the availability of lasers and the potential for massive parallelism [3]. However, diffraction precludes light from patterning features smaller than $\lambda/(2NA)$, the so-called Abbé or far-field diffraction limit when using conventional imaging techniques [4]. Here, NA is the numerical aperture of the imaging system.

The far-field diffraction barrier can be overcome in the near field [5]. However, the small distances involved make such approaches challenging to parallelize, which is essential for high speed. Two-photon lithography can also overcome this limit, but at the cost of very high light intensities [6]. Recently, two alternate methods that have the potential to overcome the diffraction limit in the far field have been proposed. These methods both rely on the exposure of a node, which was first demonstrated in atom lithography [7–10]. The first method exploits the photo-induced activation and deactivation of polymerization reactions [11–14]. Photopolymerization induced within the focal volume of a first beam is deactivated except near the center by a second aligned nodal illumination. The overall effect is to limit polymerization to a region that is smaller than the width of the diffraction-limited focal spot. The nodal beam must have high intensity to efficiently deactivate the polymerization reaction before it proceeds to completion. Therefore, this approach is difficult to

parallelize. Furthermore, the poor spectral selectivity of the activation and deactivation reactions leads to low image contrast, which has so far limited this approach to patterning isolated features.

The second method, absorbance modulation [15–18], employs a layer of photochromic molecules that are placed atop a separate photoresist film. As indicated in Fig. 1(a), these molecules can be switched between two isomeric forms by illumination at two wavelengths. When the photochromic film is simultaneously exposed to a spot at one wavelength (λ_1) and a node at another wavelength (λ_2), it is possible to spatially localize one of the isomers within a narrow region in the vicinity of the node. Since this isomer is more transparent to λ_1 compared to the other, the transmitted light at λ_1 is localized to the same narrow region, and can be recorded in the underlying photoresist. This approach is currently limited by the low quantum efficiency of one of the two photoreactions. This, in turn, necessitates high intensity in the nodal beam.

Microscopy beyond the far-field diffraction limit has been enabled by saturating an optical transition such as fluorescence [19]. It was also proposed that if this saturated transition was coupled with a “locking” step, optical nanopatterning would be possible [20]. Here, we report an implementation of this idea, which we call patterning via optical-saturable transitions (POST). In the current implementation of POST, the recording medium is a photochromic film composed of 1, 2-bis(5, 5'-dimethyl-2, 2'-bithiophen-yl) perfluorocyclopent-1-ene (compound 1) shown in Fig. 1(a) [21].

Compound 1 exists in two isomeric forms, open-ring (1o) and closed-ring (1c). Because of the extended conjugation of 1c, it can be selectively oxidized to a stable cation (1ox) as indicated in Fig. 1(a) [22]. The sequence of steps involved in POST is illustrated in Fig. 1(b). The sample is typically a silicon wafer coated with a thin platinum film and a photochromic overlayer [21]. First,

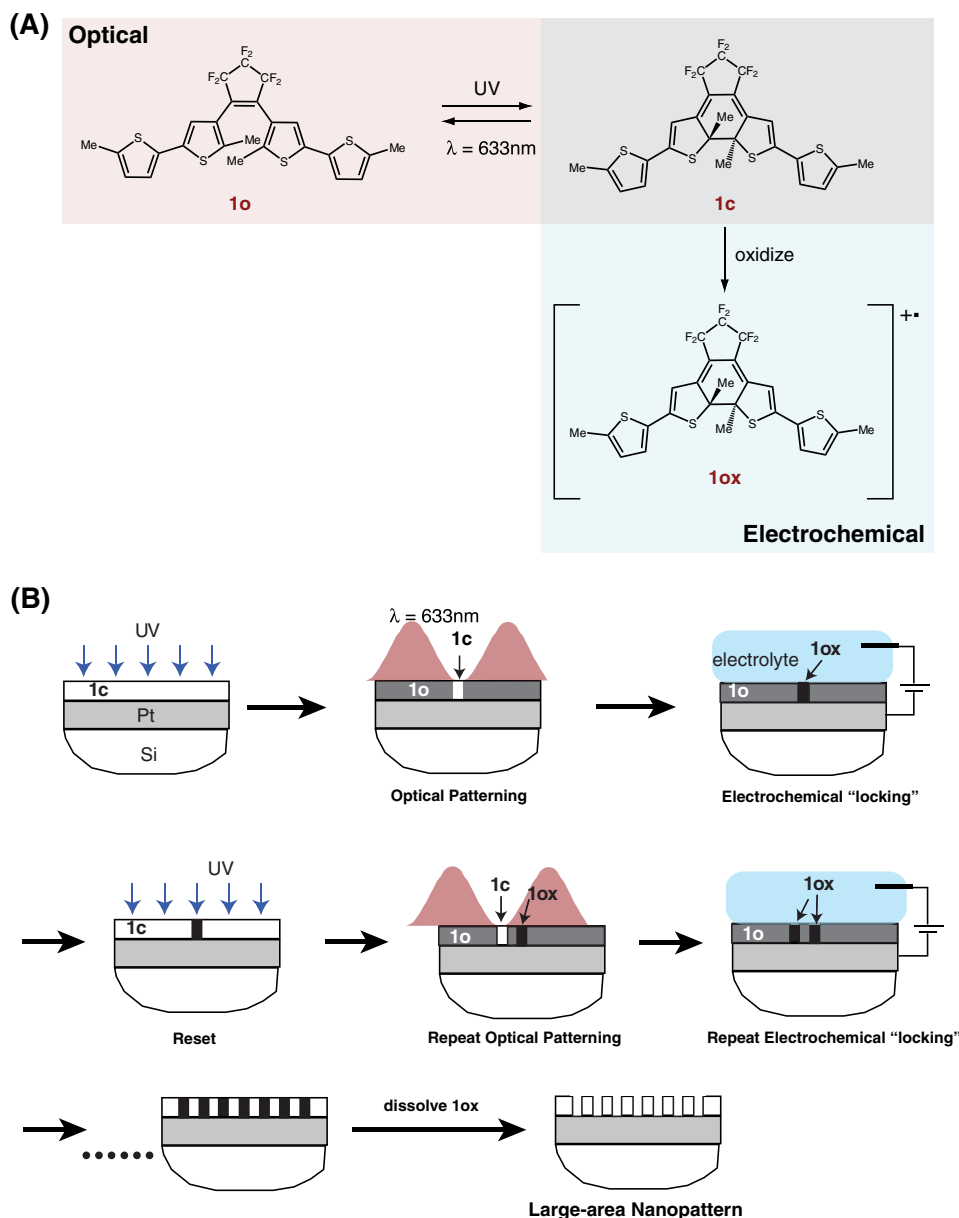


FIG. 1 (color online). Patterning via optical-saturable transitions (POST). (a) Scheme of the photochromic molecule, compound 1. (b) Sequence of steps for POST. Uniform UV illumination converts all molecules to 1c. A node at $\lambda = 633$ nm converts all molecules to 1o except at the node, where they remain in 1c. In other words, by saturating the photochemical transition from 1c to 1o, we can confine the molecules in 1c to a subwavelength region at the node. A subsequent electrochemical oxidation step converts only those molecules remaining in form 1c into the stable radical cation, 1ox. Note that 1ox is not photochromic, and therefore does not participate in any further photo-reactions. The three steps are repeated with intervening displacements of the sample, as illustrated. This leads to regions of 1ox interspersed within the layer of 1o. After all the exposures are completed, the regions of 1ox are selectively dissolved away in a polar solvent. The remaining film could serve as a resist to a subsequent pattern-transfer step [23,24]. With POST, the spacing between the features is limited primarily by the quality of the node and not by

the molecules are converted to 1c by uniform illumination with a short-wavelength UV lamp (UVP UVGL-25). Then, the sample is exposed to a nodal illumination at $\lambda = 633$ nm (Melles-Griot 05-LHP-151). This converts all the molecules to 1o except in the vicinity of the node, where they remain in 1c. In other words, by saturating the photochemical transition from 1c to 1o, we can confine the molecules in 1c to a subwavelength region at the node. A subsequent electrochemical oxidation step converts only those molecules remaining in form 1c into the stable

radical cation, 1ox. Note that 1ox is not photochromic, and therefore does not participate in any further photo-reactions. The three steps are repeated with intervening displacements of the sample, as illustrated. This leads to regions of 1ox interspersed within the layer of 1o. After all the exposures are completed, the regions of 1ox are selectively dissolved away in a polar solvent. The remaining film could serve as a resist to a subsequent pattern-transfer step [23,24]. With POST, the spacing between the features is limited primarily by the quality of the node and not by

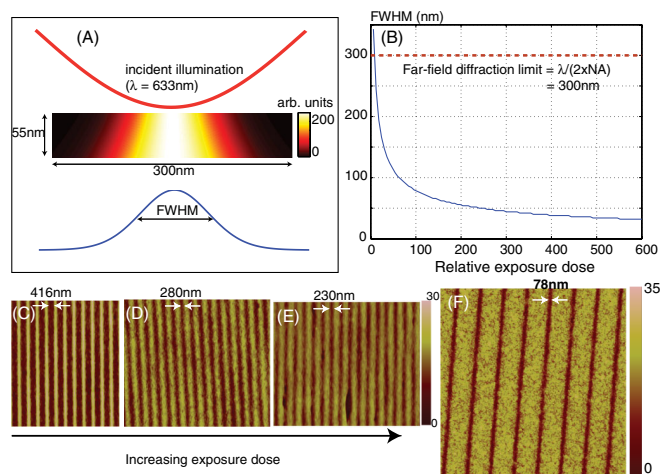


FIG. 2 (color online). Simulation and electrochemical characterization of POST. (a) Simulated distribution of 1ox at the end of a single-exposure-oxidation cycle. The incident illumination is a standing wave of period 600 nm ($\lambda = 633$ nm). The cross section of the 1ox distribution at the top of the film is shown below. (b) FWHM as a function of relative exposure dose with the same illumination conditions as in (a). (c)–(e) Atomic-force micrographs of isolated lines patterned using POST. Note that the linewidths decrease with increasing exposure dose. (f) Atomic-force micrograph of isolated lines of width 78 nm. Experimental details are provided in the text.

diffraction. Furthermore, the two isomers are thermally stable and only single-photon reactions are involved. This allows for high resolution at low light intensities.

The simulated distribution of the relative concentration of 1ox after a single-exposure–oxidation cycle is shown in Fig. 2(a) [21]. Material properties of compound 1 as well as an incident standing wave at $\lambda = 633$ nm with a period of 600 nm were assumed. 1ox is primarily localized to a small region at the node of the illumination. The distribution

shows a unique undercut profile, which was experimentally verified as described later. In POST, the “node” is recorded to create the feature. Hence, the feature size decreases with increasing exposure dose. This is simulated in Fig. 2(b), where the full-width at half-maximum (FWHM) of the distribution of 1ox at the top of the layer is plotted as a function of the relative exposure dose. Note that the FWHM decreases beyond the far-field diffraction limit of the simulated system, i.e., 300 nm. In fact, the smallest achievable width is limited primarily by the quality of the node. Figures 2(c) and 2(d) show that the linewidths decrease as the exposure dose is increased. Lines as small as 78 nm were also resolved as shown in Fig. 2(f). Further details of the experiments are given below.

Cyclic voltammograms (CVs) of both isomers in dichloromethane (DCM), shown in Fig. 3(a), confirmed that the first oxidation peak of the closed form occurs at 0.97 V (vs Ag/AgCl), which is 0.3 V lower than the first oxidation peak of the open form [21]. At 0.97 V the closed form is preferentially oxidized into a stable radical cation [25]. Thin films of 1c deposited on platinum or ITO electrodes were oxidized by immersing in purified water with platinum or ITO as the working electrode, a platinum wire counter electrode, and a Ag/AgCl reference electrode [21]. Thin films of 1c, 1o, and 1ox were further characterized via ultraviolet-visible (UV-Vis) absorption spectroscopy [Fig. 3(b)]. The spectra confirm the existence of three distinct and stable states (also evident by their distinct colors in the optical micrographs).

For patterning experiments, we thermally evaporated 45 to 55 nm thick layers of compound 1 at 73 °C onto a substrate composed of 100 nm of platinum on a silicon wafer. Then, samples were irradiated with short-wavelength UV light for about 5 min to fully convert the film to 1c. A Lloyd’s-mirror interferometer with a helium-neon laser was used to generate a standing wave with a

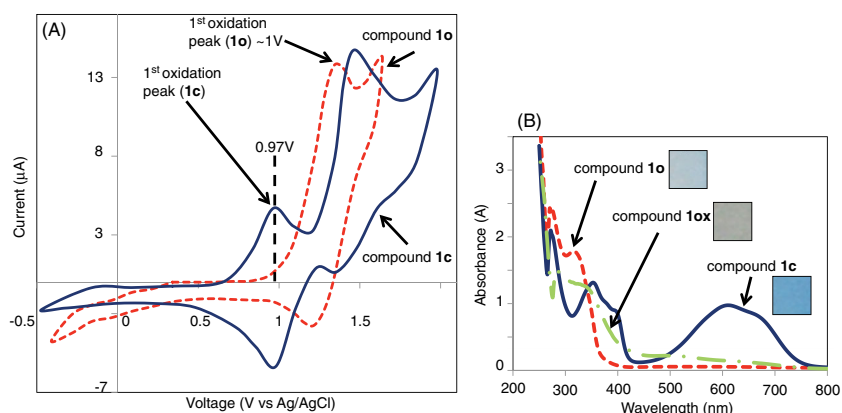


FIG. 3 (color online). Characterization of the three isomeric forms of compound 1. (a) Cyclic voltammograms of both open and closed isomers in solution (0.3 mM compound 1 in 0.1 M TBAPF₆ in DCM, platinum button working electrode, 100 mV/sec). The closed form is oxidized at 0.97 V while the open form is oxidized at 1.28 V. (b) UV-Vis absorbance curves of 80 nm of compound 1 thermally evaporated onto an ITO-coated glass slide show clear distinctions between the three forms. Optical micrographs of the three forms (insets) also show distinct colorations.

period of ~ 610 nm [21]. After exposure, the sample was electrochemically oxidized at V_{ox} for 10 min in an electrolyte with the platinum layer as the working electrode, a platinum wire counter electrode, and a Ag/AgCl reference electrode. The peak oxidation voltage V_{ox} was determined by performing cyclic voltammetry on a test sample from each evaporation batch, and it varied between 0.9 and 1.1 V. The electrolyte was either purified water or a dilute NaCl solution. Finally, the sample was developed in a mixture of 5% isopropyl alcohol and 95% ethylene glycol by volume for 60 s.

The lines in Figs. 2(c)–2(e) were exposed with an incident power density of 4.5 mW/cm² and exposure times of 30, 45, and 50 min, respectively. The samples were oxidized at 0.93 V for 10 min and finally developed as usual. Isolated lines with widths as narrow as 78 nm (or $\lambda/8$) were clearly resolved with a single exposure as illustrated in the atomic-force micrograph in Fig. 2(f). In this case, the exposure time was 315 s at an incident intensity of ~ 45 mW/cm². This particular sample was oxidized at $V_{\text{ox}} = 1.08$ V for 10 min in a 0.04M NaCl solution. Figure 4(a) shows a two-step exposure where the sample was rotated by about 25° between the exposures. The exposure time for each step was 45 min at an incident intensity of 4.5 mW/cm². The sample was exposed to the short-UV lamp for 6 min after the first exposure and oxidation. The oxidation conditions were $V_{\text{ox}} = 0.91$ V for 5 min in purified water. Finally, the sample was developed as usual. As indicated in the top schematic, this dual-exposure process should result in a crossed-line pattern, where the spacing between adjacent lines decrease to zero. The corresponding atomic-force micrograph in Fig. 4(b) resolves lines with spacing as small as 153 nm

or $\lambda/4$, about half the far-field diffraction limit. On a separate sample, we performed two consequent exposures (exposure time = 67 min each, incident intensity = 4.5 mW/cm²) with intervening oxidation steps ($V_{\text{ox}} = 1.1$ V for 10 min each in purified water). The sample was exposed to the UV lamp for 6 min before the second exposure. In this case, the sample was removed from the exposure system for the oxidation step. When it was placed back in the exposure system for the second exposure, random displacements were introduced. After the final dissolution step, the sample was examined thoroughly, and a portion is shown in the atomic-force micrograph in Fig. 4(b). The spacing between the lines is 263 nm, which is less than half the far-field diffraction limit of $\lambda/(2\text{NA}) = 610$ nm. Figure 4(c) shows a scanning-electron micrograph of the cross section of a single-exposure line of width 89 nm. This sample was exposed for 65 min at an incident power of 4.5 mW/cm², and oxidized at $V_{\text{ox}} = 0.93$ V for 10 min in purified water. The undercut feature, which was predicted by the simulations in Fig. 2(a) is confirmed as shown in Fig. 4(d). This feature could be advantageous for pattern transfer using lift-off. The patterned area in all these samples was limited by the width of the incident beam, and uniform lines were observed over areas as large as 0.5 mm² (corresponding approximately to a semicircle of radius 0.6 mm).

It must be noted that in the semiconductor industry, lithography is currently performed with ~ 70 nm spacing between features [26]. This is achieved using a diffraction-limited image-replication process that utilizes 193 nm illumination wavelength under water immersion. The original pattern is typically created via scanning-electron-beam lithography, which is too slow for manufacturing.

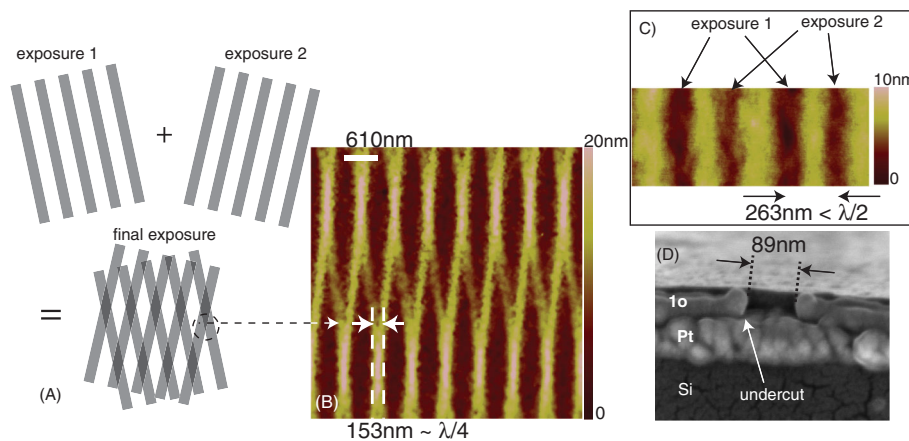


FIG. 4 (color). Experimental confirmation of sub-diffraction-limited optical nanopatterning. (a) Two-step exposure process where the sample is rotated in between the exposures. An intervening oxidation step “fixes” the first exposed pattern such that it is minimally perturbed by the next exposure. A 6-min UV exposure is used to bring all the molecules back to the open state before the second exposure. (b) Atomic-force micrograph of the final pattern agrees well with the expected pattern. The smallest resolved spacing between features is about 153 nm. (c) Atomic-force micrograph of a sample that underwent two exposures. The spacing between the lines is 263 nm, which is less than half the far-field diffraction limit in this case (610 nm). (d) Cross-section scanning-electron micrograph of a single-exposure line of width 89 nm. The undercut predicted by the simulation in Fig. 2(a) is clearly observed. The experimental details are described in the text.

In order to replicate patterns at even smaller feature spacings, shorter wavelengths are necessary, which give rise to enormous challenges in implementation [27]. Alternative proposals rely on massively parallel electron beams with their concomitant disadvantages [28]. POST offers an elegant alternative with the promise of relatively fast, large-area diffraction-unlimited nanopatterning with low-cost UV lamps and visible-light sources.

In conclusion, we demonstrated optical patterning of isolated lines as small as $\lambda/8$ and adjacent features spaced by as small as $\lambda/4$ with single-photon transitions (low light intensities) and simple electrochemistry. Improved illumination conditions and materials optimization should enable scaling of features far below 100 nm. Our approach opens the door to high-speed large-area nanopatterning via parallelism. An array of independently controllable nodes can enable parallel patterning of complex geometries in a “dot-matrix” fashion [29]. Although the current demonstration utilized one-dimensional standing waves, we anticipate straightforward extension to two- and three-dimensional patterning using either diffractive optics [30–32] or phase masks [33].

We thank Deborah Mascaro for use of the low-temperature evaporator, Jennifer Schumaker-Perry for use of the UV-Vis spectrometer, Mohit Diwekar for assistance with platinum sputtering, Brian Van Devener for assistance with atomic-force microscopy, Randy Polson for assistance with scanning-electron microscopy, and Brian Baker, Paul Cole, and Charles Fisher for help in the Utah microfabrication facility. N.B. and R.V.M. were supported by the Utah Science Technology and Research (USTAR) initiative. R.V.M. was partially supported by a DARPA Contract No. N66001-10-1-4065. R.M. gratefully acknowledges support from the NSF.

*rmenon@eng.utah.edu

- [1] K. Murooka, K. Hattori, and O. Iizuka, *J. Vac. Sci. Technol. B* **21**, 2668 (2003).
- [2] J. T. Hastings, F. Zhang, and H. I. Smith, *J. Vac. Sci. Technol. B* **21**, 2650 (2003).
- [3] H. I. Smith, R. Menon, A. Patel, D. Chao, M. Walsh, and G. Barbastathis, *Microelectron. Eng.* **83**, 956 (2006).
- [4] E. Abbé, *Arch. Mikrosk. Anat. Entwicklunsmech.* **9**, 413 (1873).
- [5] E. A. Ash and G. Nichols, *Nature (London)* **237**, 510 (1972).
- [6] S. Kawata, H. B. Sun, T. Tanaka, and T. Takada, *Nature (London)* **412**, 697 (2001).
- [7] K. K. Berggren, A. Bard, J. L. Wilbur, J. D. Gillaspay, A. G. Helg, J. J. McClelland, S. L. Rolston, W. D. Phillips, M. Prentiss, and G. M. Whitesides, *Science* **269**, 1255 (1995).
- [8] U. Drodofsky, J. Stuhler, B. Brezger, Th. Schulze, M. Drewsen, T. Pfau, and J. Mlynek, *Microelectron. Eng.* **35**, 285 (1997).
- [9] Th. Schulze, B. Brezger, R. Mertens, M. Pivk, T. Pfau, and J. Mlynek, *Appl. Phys. B* **70**, 671 (2000).
- [10] M. K. Oberthaler and T. Pfau, *J. Phys. Condens. Matter* **15**, R233 (2003).
- [11] J. T. Fourkas, *J. Phys. Chem. Lett.* **1**, 1221 (2010).
- [12] L. J. Li, R. R. Gattass, E. Gershgoren, H. Hwang, and J. T. Fourkas, *Science* **324**, 910 (2009).
- [13] T. F. Scott, B. A. Kowalski, A. C. Sullivan, C. N. Bowman, and R. R. McLeod, *Science* **324**, 913 (2009).
- [14] J. Fischer, G. von Freymann, and M. Wegener, *Adv. Mater.* **22**, 3578 (2010).
- [15] T. L. Andrew, H-Y. Tsai, and R. Menon, *Science* **324**, 917 (2009).
- [16] R. Menon and H. I. Smith, *J. Opt. Soc. Am. A* **23**, 2290 (2006).
- [17] R. Menon, H-Y. Tsai, and S. W. Thomas III, *Phys. Rev. Lett.* **98**, 043905 (2007).
- [18] H-Y. Tsai, G. W. Walraff, and R. Menon, *Appl. Phys. Lett.* **91**, 094103 (2007).
- [19] S. W. Hell, *Science* **316**, 1153 (2007).
- [20] S. W. Hell, *Phys. Lett. A* **326**, 140 (2004).
- [21] See Supplemental Material at <http://link.aps.org/supplemental/10.1103/PhysRevLett.107.205501> for further information.
- [22] T. Saika, M. Irie, and T. Shimidzu, *J. Chem. Soc. Chem. Commun.* **1994**, 2123 (1994).
- [23] T. Ito, T. Yamada, Y. Inao, T. Yamaguchi, N. Mizutani, and R. Kuroda, *Appl. Phys. Lett.* **89**, 033113 (2006).
- [24] D. Pires, J. L. Hedrick, A. De Silva, J. Frommer, B. Gotsmann, H. Wolf, M. Despont, U. Duerig, and A. W. Knoll, *Science* **328**, 732 (2010).
- [25] W. R. Browne, J. J. D. de Jong, T. Kudernac, M. Walko, L. N. Lucas, K. Uchida, J. H. van Esch, and B. L. Feringa, *Chem. Eur. J.* **11**, 6430 (2005).
- [26] International Technology Roadmap for Semiconductors, <http://public.itrs.net/>.
- [27] E. S. Putna, T. R. Younkin, M. Leeson, R. Caudillo, T. Bacuita, U. Shah, and M. Chandhok, *Proc. SPIE Int. Soc. Opt. Eng.* **7969**, 79692K (2011).
- [28] R. Freed, J. Sun, A. Brodie, P. Petric, M. McCord, K. Ronse, L. Haspelslagh, and B. Vereecke, *Proc. SPIE Int. Soc. Opt. Eng.* **7970**, 79701T (2011).
- [29] R. Menon, A. A. Patel, D. Gil, and H. I. Smith, *Mater. Today* **8**, 26 (2005).
- [30] H-Y. Tsai, H. I. Smith, and R. Menon, *J. Vac. Sci. Technol. B* **25**, 2068 (2007).
- [31] H-Y. Tsai, H. I. Smith, and R. Menon, *Opt. Lett.* **33**, 2916 (2008).
- [32] H-Y. Tsai, S. W. Thomas III, and R. Menon, *Opt. Express* **18**, 16 014 (2010).
- [33] S. W. Hell, R. Schmidt, and A. Egner, *Nat. Photon.* **3**, 381 (2009).